The Astrophysical Journal, 682:1392–1403, 2008 August 1

A THREE-DIMENSIONAL MULTILAYERED SPHERICAL DYNAMIC INTERFACE DYNAMO USING THE MALKUS-PROCTOR FORMULATION

K. H. Chan
Department of Mathematics, University of Hong Kong, Pokfulam, Hong Kong, China; mkhchan@hku.hk
X. Liao
Shanghai Astronomical Observatory, Shanghai 200030, China; xhliao@shao.ac.cn
and
K. Zhang
Center for Geophysical and Astrophysical Fluid Dynamics, and Department of Mathematical Sciences, University of Exeter, Exeter EX4 4QE, UK; kzhang@ex.ac.uk
Received 2007 September 26; accepted 2008 March 31

ABSTRACT

We investigate a fully three-dimensional and multilayered spherical dynamic interface dynamo using a finite-element method based on the three-dimensional tetrahedralization of the whole spherical system. The dynamic interface dynamo model consists of four magnetically coupled zones: an electrically conducting and uniformly rotating core, a thin differentially rotating tachocline, a turbulent convection envelope, and a nearly insulating exterior. In the thin tachocline at the base of the convection zone, a differential rotation, similar to that of the observed solar differential rotation, is imposed. In the convection zone, the Malkus-Proctor formulation with a prescribed α-effect is employed while the fully three-dimensional dynamic feedback of Lorentz forces is taken into account. Our numerical simulations of the dynamic interface dynamo are focused on the Taylor number $\mathrm{Ta} = 10^5$ with a unity magnetic Prandtl number. It is shown that the dynamic interface dynamo, depending on the size of the magnetic Reynolds number Re_m based on the differential rotation, can be either nonaxisymmetric or axisymmetric. When Re_m is small or moderate, the dynamic dynamo is characterized by quasi-periodic and nonaxisymmetric azimuthally traveling waves. When Re_m is sufficiently large, the dynamo is characterized by a strong toroidal magnetic field, axisymmetric or nearly axisymmetric, that selects dipolar symmetry and propagates equatorward. Implications of our dynamic interface dynamo for the solar dynamo are also discussed.

Subject heading: Sun: magnetic fields

1. INTRODUCTION

Regular global-scale solar magnetic activities, such as the 11 yr sunspot cycle, reflect the complex magnetohydrodynamic processes occurring in the deep solar interior (Weiss 1994). In particular, it is widely believed that the solar tachocline, a highly differentially rotating transition zone between the convection envelope and radiative core of the Sun, plays a critical role (e.g., Parker 1993; Kosovichev 1996). Significant progress has been made, via both observations and numerical modeling, in the understanding of the magnetohydrodynamic processes taking place in the solar interior (e.g., Brandenburg & Subramanian 2005; Charbonneau 2005; Zhang & Schubert 2006).

Numerical modeling of the solar magnetohydrodynamic processes has mainly focused on the five different aspects: (1) fully three-dimensional spherical shell simulations of convection-driven dynamos dealing with various aspects of the problem (e.g., Glatzmaier & Gilman 1982; Brun & Toomre 2002; Miesch et al. 2008), for example, an attempt to understand turbulent convection penetration downward into a tachocline of rotational shear (Browning et al. 2006); (2) high-resolution simulations in the localized planar domain aimed at understanding the basic hydrodynamic and magnetohydrodynamic processes (e.g., Tobias 1997; Cattaneo 1999; Brandenburg 2001; Cline et al. 2003; Liao & Zhang 2006; Liao et al. 2007); (3) the kinematic mean field approach in attempting to elucidate the mechanism of the solar interface dynamo (e.g., Parker 1993; Charbonneau & MacGregor 1997; Markiel & Thomas 1999; Dikpati & Charbonneau 1999; Zhang et al. 2003; Bushby 2003); (4) the kinematic mean field approach using the previous solar cycle's data in predicting the future of an upcoming solar cycle (e.g., Dikpati et al. 2006; Dikpati & Gilman 2006; Cameron & Schüssler 2007); and (5) the dynamic mean field approach taking into account the feedback of an axisymmetric Lorentz force (e.g., Covas et al. 2001; Rempel 2006a, 2006b). These studies paint an increasingly clearer picture of how the solar dynamo may operate. Highly turbulent convective motions in the convection zone produce an α-effect generating a weak magnetic field which either diffuses or is transported into the tachocline at the base of the convection zone. The highly differentially rotating tachocline, with a reduced magnetic diffusivity, generates strong toroidal magnetic fields propagating toward the equator. When the strong azimuthal fields stored in the tachocline become unstable as a result of magnetic buoyancy, the toroidal magnetic fields buckle and twist, eventually rising and forming Ω-shaped loops, intersecting the Sun's surface to produce the magnetic active regions and sunspots.

This work is the second paper in a series reporting our attempt to construct a three-dimensional, multilayered, finite-element *solar interface dynamo model*. In the first paper (Zhang et al. 2003), we described the numerical scheme and finite-element formulation of the three-dimensional kinematic interface dynamo, and we also computed the kinematic interface dynamo. There exist two important features in the kinematic interface dynamo discussed in the first paper (Zhang et al. 2003): (1) neither spatial nor temporal symmetries are imposed in the kinematic dynamo solutions and (2) both the radiative core and the exterior to the convection

zone, magnetically coupled to the magnetic field generation regions, are solved as part of the kinematic dynamo solution. It was found that the three-dimensional kinematic interface dynamo is capable of producing an oscillatory dynamo with a period of about 20 yr, selecting dipolar symmetry, and propagating equatorward, even though the numerical simulation is fully three-dimensional.

The primary objective of the present work is to extend the previous kinematic interface dynamo to the dynamic regime by considering the fully three-dimensional feedback of Lorentz forces in the convection zone using the Malkus-Proctor formulation (Malkus & Proctor 1975) in the absence of thermal convection. In comparison to the kinematic dynamo problem, the dynamic interface dynamo requires not only an additional equation of motion, but also additional physical parameters, such as the Taylor number Ta, pertaining to the dynamic problem in rotating fluid systems. Furthermore, we have modified our existing numerical scheme (Zhang et al. 2003) by introducing an element-by-element (EBE) finite-element method capable of taking full advantage of modern massively parallel computers, leading to an effective parallelization achieving nearly linear scalability on parallel computers. It should also be mentioned that our EBE finite-element dynamo code has been carefully compared with the well-known benchmark dynamo using spectral methods, showing a satisfactory agreement between two fundamentally different models (Chan et al. 2007). Following the basic interface dynamo concept of Parker (1993; see also MacGregor & Charbonneau 1997), we shall assume a separation between the α-effect and shear flow regions: the convectional α-effect is nonzero only in the convection zone, while the differential rotation occurs only in the tachocline. This allows the two magnetic induction sources to be isolated and identified by switching on or off the action of the tachocline, and hence offers helpful insight into the interface generation mechanism. But the explicit effect of the thermal convection and heat equation is neglected in this interface dynamo model. It is also worth mentioning one major difference between the current 3D interface dynamo and the axisymmetric dynamo by Rempel (2006b). In the present model, the three-dimensional flow cells are able to generate the differential rotation via the Reynolds stresses, while the effects of the latitudinal entropy gradient are absent.

Our numerical simulations of the dynamic interface dynamo are focused on the Taylor number $\mathrm{Ta} = 10^5$ which is chosen because it is close to the value of the Taylor number in the solar convection zone if an appropriate turbulent viscosity is employed and because it is sufficiently large to have substantial rotational effects on the dynamics of the convection zone. It was shown (e.g., Brandenburg et al. 1992) that the rotational effects would generate the Taylor cylindrical contours of the angular velocity which cannot be altered by the effects of stratification and compressibility. Later studies suggest that thermal effects, for example via the latitudinal entropy gradient, may play an important role in changing the profile of the differential rotation from being cylindrical to conical (e.g., Kitchatinov & Rüdiger 1995; Rempel 2006b). However, since our primary aim is at providing an improved understanding of the basic magnetic field generation process in the *three-dimensional spherical dynamic interface dynamo* using the Malkus-Proctor formulation, the issue of the Taylor number puzzle is beyond the scope of the present study.

The remainder of the paper is organized as follows. After discussing the mathematical formulation of the problem for the dynamic interface dynamo in § 2, § 3 presents the results of our three-dimensional dynamic dynamo simulations. Section 4 closes the paper with a summary and some remarks.

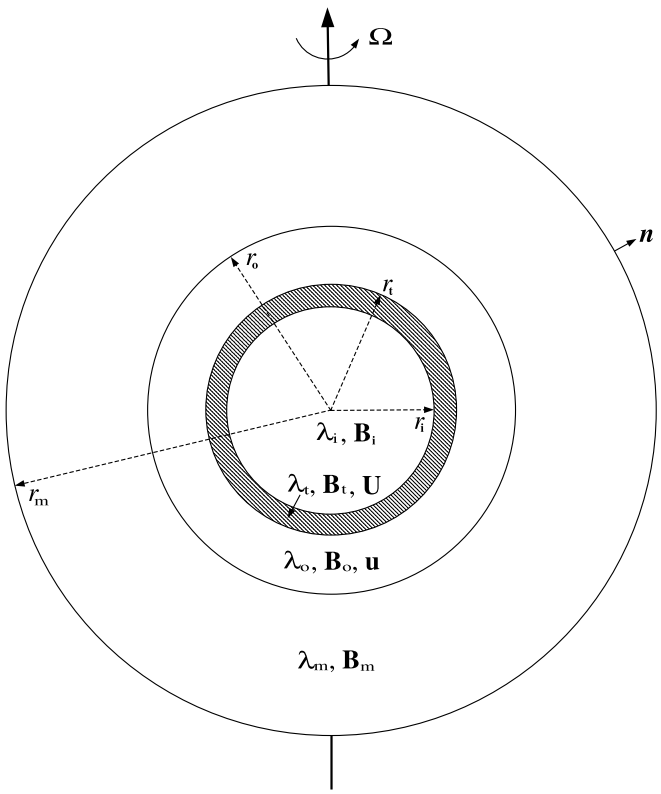

FIG. 1.—Geometry of the three-dimensional, four-zone, dynamic-interface dynamo model: $0 < r \le r_i$, the uniformly rotating, electrically conducting core with magnetic diffusivity λ_i; $r_i \le r \le r_t$, the differentially rotating tachocline with magnetic diffusivity λ_t; $r_t \le r \le r_o$, the convection zone with magnetic diffusivity λ_o; and $r > r_o$, the exterior with large magnetic diffusivity λ_e.

2. MATHEMATICAL FORMULATION

Our spherical dynamic interface dynamo consists of four different zones, as illustrated in Figure 1. The inner radiative sphere, $0 < r < r_i$, with constant magnetic diffusivity λ_i, is assumed to rotate uniformly with the angular velocity $\boldsymbol{\Omega}$. If we also adopt a reference frame that rotates with $\boldsymbol{\Omega}$, the magnetic field $\boldsymbol{B}_i$ in the radiative core is governed by the equations

$$\frac{\partial \boldsymbol{B}_i}{\partial t} + \lambda_i \nabla \times \nabla \times \boldsymbol{B}_i = 0, \tag{1}$$

$$\nabla \cdot \boldsymbol{B}_i = 0. \tag{2}$$

Note that the magnetic field $\boldsymbol{B}_i$ cannot be generated in this uniformly rotating radiative core assumed in the present model although the magnetic field can be diffused into it. In reality, the radiative core is not static and may be able to sustain dynamo action (Spruit 2002; Zahn et al. 2007). Above the radiative core is the tachocline, a stably stratified region of strong differential rotation, $\boldsymbol{\Omega}_0 \Omega_t$, where $\boldsymbol{\Omega}_0$ is in the same direction as $\boldsymbol{\Omega}$, $|\boldsymbol{\Omega}_0|$ is the amplitude of the differential rotation, and Ω_t is the dimensionless profile. In the tachocline $r_i < r < r_t$, the magnetic diffusivity λ_t is reduced and the differential rotation shears the weak poloidal magnetic field that is generated in the convection zone and that penetrates into the tachocline. The result is a strong magnetic field $\boldsymbol{B}_t$ in the tachocline, with the amplification process described by the equations

$$\frac{\partial \boldsymbol{B}_t}{\partial t} = \nabla \times (\boldsymbol{U} \times \boldsymbol{B}_t) - \lambda_t \nabla \times \nabla \times \boldsymbol{B}_t, \tag{3}$$

$$\nabla \cdot \boldsymbol{B}_t = 0, \tag{4}$$

where

$$\boldsymbol{U} = \Omega_t(r,\theta)\boldsymbol{\Omega}_0 \times \boldsymbol{r} = |\boldsymbol{\Omega}_0|\Omega_t(\theta) r \sin\theta \sin\left[\pi \frac{(r-r_i)}{(r_t-r_i)}\right]\hat{\phi}, \quad (5)$$

where $\boldsymbol{r}$ is the position vector and $\Omega_t(\theta)$ represents the three-term expression approximating the observed profile of the solar differential rotation (e.g., Schou et al. 1998),

$$\Omega_t(\theta) = 1 - 0.1264\cos^2\theta - 0.1591\cos^4\theta.$$

In our dynamo model, we do not impose the pole-equator differential rotation in the convection zone which is generated dynamically through the action of both the Reynolds stresses and the Lorentz forces. The differential rotation, which is imposed in the tachocline, vanishes at the interface $r = r_t$ so as to spatially separate the two magnetic induction sources (Parker 1993; MacGregor & Charbonneau 1997). An unsolved problem in the solar dynamo is concerned with how and why the tachocline is formed at the base of the convection zone (Zhang & Schubert 2006). In the present model, the shear flow in the thin tachocline is prescribed, essentially providing the boundary condition required for the dynamical dynamo problem in the convection zone. Since we do not really know the formation mechanism of the tachocline and since the tachocline shear is prescribed in the first place, we shall neglect the dynamic effects in both the stably stratified radiative core and tachocline. It is worth noting that, without α-effects in the convection zone, dynamo action in this multilayer system cannot be sustained by a purely toroidal axisymmetric flow within the tachocline: a key ingredient in the Parker's interface dynamo.

We assume a fully turbulent convection zone in the region $r_t < r < r_o$ in which both the Coriolis force and the Lorentz force play a significant role in the dynamic interface dynamo. Similar to the previous dynamo models (Covas et al. 2001; Rempel 2006b), we shall model small-scale turbulence by assuming an eddy magnetic diffusivity λ_o with an assumption that $\lambda_t/\lambda_o \ll 1$ and an eddy viscosity ν_o giving rise to a moderate Taylor number. A weak mean magnetic field $\boldsymbol{B}_o$ is generated by the prescribed α-effect in the fully turbulent convection zone. The equation of motion governing the flow velocity $\boldsymbol{u}$ and the generated magnetic field $\boldsymbol{B}_o$ in the convection zone is

$$\frac{\partial \boldsymbol{u}}{\partial t} + \boldsymbol{u}\cdot\nabla\boldsymbol{u} + 2\Omega\boldsymbol{k}\times\boldsymbol{u} = -\frac{1}{\rho}\nabla p + \frac{1}{\rho\mu}(\nabla\times\boldsymbol{B}_o)\times\boldsymbol{B}_o + \nu_o\nabla^2\boldsymbol{u}, \quad (6)$$

where $\boldsymbol{k}$ is a unit vector parallel to the axis of rotation, along with the condition of assumed incompressibility given by

$$\nabla\cdot\boldsymbol{u} = 0. \quad (7)$$

The dynamo equations in the convection zone are

$$\frac{\partial \boldsymbol{B}_o}{\partial t} = \alpha_0\nabla\times\left[\alpha\left(r,\theta,\phi,|\boldsymbol{B}_o|^2\right)\boldsymbol{B}_o\right] + \nabla\times(\boldsymbol{u}\times\boldsymbol{B}_o) - \lambda_o\nabla\times\nabla\times\boldsymbol{B}_o, \quad (8)$$

$$\nabla\cdot\boldsymbol{B}_o = 0. \quad (9)$$

In the above equations, α_0 is a positive parameter and the three-dimensional nonlinear function $\alpha(r,\theta,\phi,|\boldsymbol{B}_o|^2)$ is related to the local α-quenching, which will be discussed further. In the convection zone, the magnetic field $\boldsymbol{B}_o$, generated by small-scale turbulence and amplified by the shear flow in the tachocline, produces the Lorentz force which, along with the Coriolis force, drives the large-scale flow $\boldsymbol{u}$, which in turn modifies the dynamo processes generating $\boldsymbol{B}_o$. In other words, a fully turbulent background state is implicitly assumed such that we are only concerned about the large-scale flow $\boldsymbol{u}$, pressure p, and magnetic field $\boldsymbol{B}_o$ generated by the relevant dynamo instabilities (Parker 1993; Covas et al. 2001). The velocity boundary condition at both the bounding surfaces is assumed to be no-slip. While the no-slip condition at $r = r_t$ is physically appropriate for an interface dynamo, it is assumed at the outer surface $r = r_o$ for numerical convenience. By choosing the no-slip condition at the base of the convection zone, we focus on the magnetic coupling between the highly turbulent convection zone generating a weak magnetic field and the highly differentially rotating tachocline producing strong toroidal magnetic fields, a primary element in the Parker's interface dynamo. Since the main dynamo activities take place in the vicinity of the tachocline, we do not expect that the type of velocity condition at $r = r_o$ is of primary importance. By neglecting the effect of the weak differential rotation in the convection zone, the dynamo problem in the convection zone is dynamically self-consistent in the framework of the Malkus-Proctor formulation which is capable of generating large-scale circulation like the differential rotation.

The exterior to the convection zone, $r_o < r \le r_m$, is assumed to be nearly electrically insulating with a large magnetic diffusivity λ_e. The magnetic field $\boldsymbol{B}_e$ is governed by

$$\frac{\partial \boldsymbol{B}_e}{\partial t} + \lambda_e\nabla\times(\nabla\times\boldsymbol{B}_e) = 0, \qquad \nabla\cdot\boldsymbol{B}_e = 0. \quad (10)$$

For sufficiently large magnetic diffusivity λ_e such that

$$\frac{\lambda_e}{\lambda_o} \gg 1,$$

the magnetic field $\boldsymbol{B}_e$ in the exterior represents an approximate potential field which is also part of the numerical dynamo solution. It should be pointed out that, to overcome the conflict between the local nature of finite-element methods and the global nature of magnetic field boundary conditions, we have to solve the exterior zone as an integral part of the whole dynamo system; a detailed discussion on the numerical treatment of the exterior can be found in Chan et al. (2001).

We nondimensionalize length by the thickness of the convection zone $d = (r_o - r_t)$, magnetic field by $\lambda_o(\rho\mu)^{1/2}/d$, and time by the magnetic diffusion time d^2/λ_o of the convection zone. The resulting four sets of dimensionless equations for the four zones (all variables in the rest of the paper are nondimensional) are

1. The zone $0 < r < r_i$:

$$\frac{\partial \boldsymbol{B}_i}{\partial t} + \beta_i\nabla\times\nabla\times\boldsymbol{B}_i = 0, \quad (12)$$

$$\nabla\cdot\boldsymbol{B}_i = 0. \quad (13)$$

2. The zone $r_i < r < r_t$:

$$\frac{\partial \boldsymbol{B}_t}{\partial t} = \mathrm{Re}_m\nabla\times\{[\Omega_t(r,\theta)\boldsymbol{k}\times\boldsymbol{r}]\times\boldsymbol{B}_t\} - \beta_t\nabla\times\nabla\times\boldsymbol{B}_t, \quad (14)$$

$$\nabla\cdot\boldsymbol{B}_t = 0. \quad (15)$$

3. The zone $r_t < r < r_o$:

$$\frac{\partial \boldsymbol{u}}{\partial t} + \boldsymbol{u}\cdot\nabla\boldsymbol{u} + \mathrm{Pr}_m \mathrm{Ta}^{1/2}\boldsymbol{k}\times\boldsymbol{u} = -\nabla p + (\nabla\times\boldsymbol{B}_o)\times\boldsymbol{B}_o + \mathrm{Pr}_m\nabla^2\boldsymbol{u}, \quad (16)$$

$$\nabla\cdot\boldsymbol{u} = 0, \quad (17)$$

$$\frac{\partial \boldsymbol{B}_o}{\partial t} = \mathrm{Re}_\alpha \nabla\times\left[\alpha\left(r,\theta,\phi,|\boldsymbol{B}_o|^2\right)\boldsymbol{B}_o\right] + \nabla\times(\boldsymbol{u}\times\boldsymbol{B}_o) - \nabla\times\nabla\times\boldsymbol{B}_o, \quad (18)$$

$$\nabla\cdot\boldsymbol{B}_o = 0. \quad (19)$$

4. The zone $r_o < r \le r_m$:

$$\frac{\partial \boldsymbol{B}_e}{\partial t} + \beta_m\nabla\times\nabla\times\boldsymbol{B}_e = 0, \quad (20)$$

$$\nabla\cdot\boldsymbol{B}_e = 0. \quad (21)$$

There are seven nondimensional quantities that characterize the dynamic interface dynamo: the three magnetic diffusivity ratios β_i, β_t, and β_m, the magnetic alpha Reynolds number Re_α, the magnetic omega Reynolds number Re_m, the magnetic Prandtl number Pr_m, and the Taylor number Ta, which are defined by

$$\beta_i = \frac{\lambda_i}{\lambda_o}, \quad \beta_t = \frac{\lambda_t}{\lambda_o}, \quad \beta_m = \frac{\lambda_e}{\lambda_o},$$
$$\mathrm{Re}_\alpha = \frac{d\alpha_0}{\lambda_o}, \quad \mathrm{Re}_m = \frac{d^2|\boldsymbol{\Omega}_0|}{\lambda_o},$$
$$\mathrm{Pr}_m = \frac{\nu_o}{\lambda_o}, \quad \mathrm{Ta} = \left(\frac{2d^2|\boldsymbol{\Omega}|}{\nu_o}\right)^2.$$

All numerical simulations reported in this paper are performed at a fixed Taylor number $\mathrm{Ta} = 10^5$ with a unity magnetic Prandtl number $\mathrm{Pr}_m = 1$ and the magnetic diffusivity ratios at $\beta_i = \beta_t = 0.1$.

The four sets of equations are solved subject to a number of matching and boundary conditions at the interfaces. At the three interfaces of the four zones, $r = r_i$, r_t, and r_o, all components of the magnetic field and the tangential component of the electrical field are continuous. These conditions yield

$$(\boldsymbol{B}_i - \boldsymbol{B}_t) = 0 \text{ at } r = r_i,$$
$$\boldsymbol{r}\times(\beta_i\nabla\times\boldsymbol{B}_i - \beta_t\nabla\times\boldsymbol{B}_t) = 0 \text{ at } r = r_i,$$
$$(\boldsymbol{B}_t - \boldsymbol{B}_o) = 0 \text{ at } r = r_t,$$
$$\boldsymbol{r}\times(-\beta_t\nabla\times\boldsymbol{B}_t - \mathrm{Re}_\alpha\alpha\boldsymbol{B}_o + \nabla\times\boldsymbol{B}_o) = 0 \text{ at } r = r_t,$$
$$(\boldsymbol{B}_e - \boldsymbol{B}_o) = 0 \text{ at } r = r_o,$$
$$\boldsymbol{r}\times(\beta_m\nabla\times\boldsymbol{B}_e + \mathrm{Re}_\alpha\alpha\boldsymbol{B}_o - \nabla\times\boldsymbol{B}_o) = 0 \text{ at } r = r_o, \quad (22)$$

where the no-slip velocity boundary condition $\boldsymbol{u} = 0$ is used to simplify the above interface conditions. For the boundary condition at the outer bounding surface of the dynamo solution domain (see Fig. 1), $r = r_m$, an approximation must be made. Since there are no sources at infinity, i.e.,

$$\boldsymbol{B}_e = O\left(r^{-3}\right), \text{ as } r\to\infty, \quad (23)$$

we can approximate the magnetic field boundary condition at $r = r_m$ as

$$\boldsymbol{B}_e = 0, \text{ at } r = r_m, \quad (24)$$

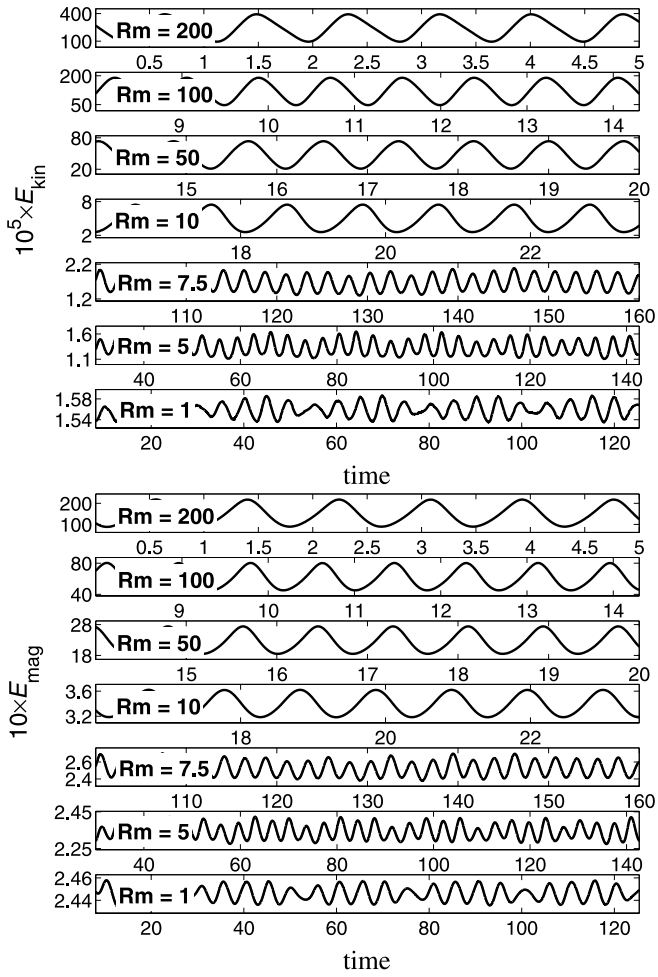

FIG. 2.—Kinetic energy E_{kin} (*top*) and magnetic energy E_{mag} (*bottom*) as a function of time for seven solutions of the dynamic interface dynamo obtained at different values of Re_m. The prescribed α is two-dimensional in the convection zone.

with $(r_m/r_o)^3 \gg 1$. Equations (12)–(21), together with the matching and boundary conditions (22) and (24), define a nonlinear dynamic interface dynamo problem. For given parameters of the dynamo model like Re_α and Re_m, numerical solutions of the dynamic interface dynamo are obtained by performing fully three-dimensional simulations on massively parallel computers.

3. MULTILAYERED SPHERICAL DYNAMIC INTERFACE DYNAMOS

3.1. *Dynamic Dynamos with 2D α-effects*

For understanding how the tachocline affects the style of dynamic interface dynamos, we start our dynamo simulations by switching off the interface effect, i.e., setting $\mathrm{Re}_m \equiv 0$ in (14). This gives rise to a conventional dynamic α^2 dynamo providing the reference state to the dynamic interface dynamo. Without the presence of the tachocline, the nonlinear dynamic dynamo is solely driven by a prescribed two-dimensional α-effect in the turbulent convection zone,

$$\alpha = \sin^2\theta\cos\theta\sin\left[\pi\frac{(r - r_t)}{(r_o - r_t)}\right] \times \frac{1}{\left(1 + |\boldsymbol{B}_o|^2\right)}, \; r_t < r \le r_o. \quad (25)$$

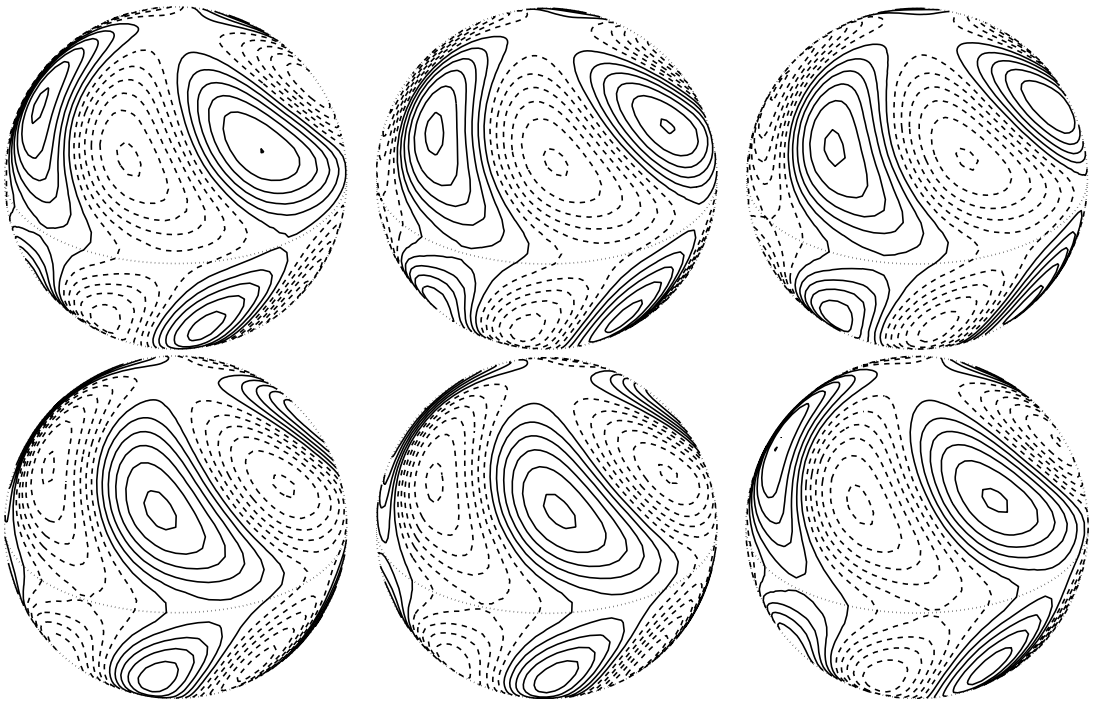

FIG. 3.—Contours of the azimuthal field B_ϕ at the base of convection zone, viewed at the angle of 30° from the axis of rotation and plotted at six different instants, $t = 108.5, 110.5, 112.0, 114.5, 115.5$, and 118.0 (*from top left to bottom right*) for $\mathrm{Re}_m = 1$ and $\mathrm{Re}_\alpha = 50$. The magnetic field is dominated by the azimuthal wavenumber $m = 3$ in the form of progradely traveling dynamo waves.

Here we have assumed that there exists an α-effect throughout the whole convection zone, but the strength of the α-effect is suppressed when the kinetic energy of the turbulent flow is comparable to the magnetic energy. A similar nonlinear quenching formula has been widely used, for example, by Choudhuri et al. (1995) and Küker et al. (2001). A major advantage of using this simple formulation is that it allows simulations of the essential large-scale processes without reference to the difficult dynamics of small-scale interaction between the flow and the Lorentz force. It should be noted that, in comparison to the kinematic dynamo problem in which the α-quenching is the only nonlinearity, there are three additional nonlinear terms in the dynamic interface

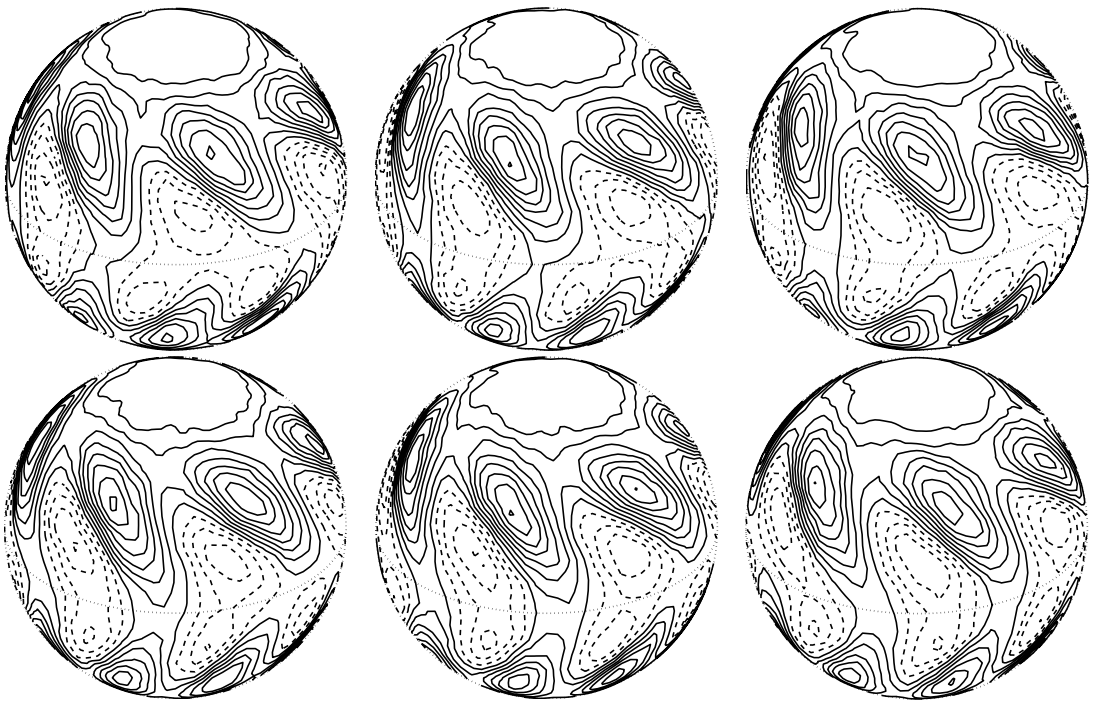

FIG. 4.—Contours of the azimuthal flow u_ϕ at the middle surface of the convection zone, viewed at the angle of 30° from the axis of rotation and plotted at six different instants, $t = 108.5, 110.5, 112.0, 114.5, 115.5$, and 118.0 (*from top left to bottom right*) for $\mathrm{Re}_m = 1$ and $\mathrm{Re}_\alpha = 50$. The velocity field is dominated by the azimuthal wavenumber $m = 6$ in the form of progradely traveling waves.

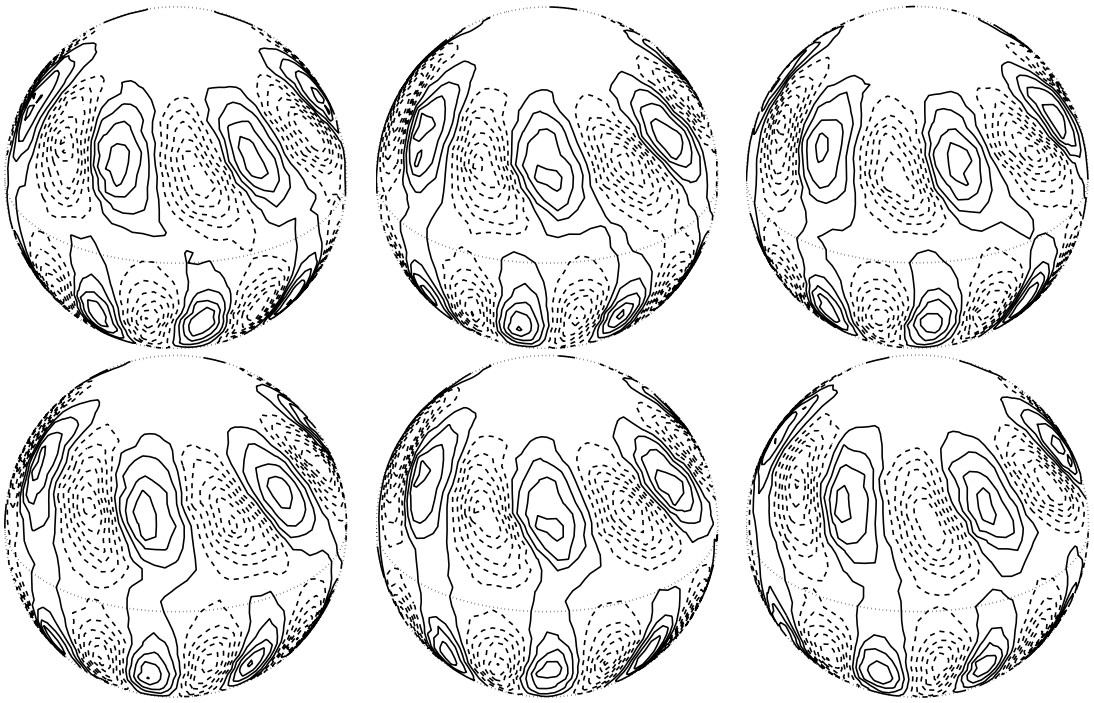

FIG. 5.—Contours of the azimuthal flow u_r at the middle surface of the convection zone, viewed at the angle of 30° from the axis of rotation and plotted at six different instants, $t = 108.5$, 110.5, 112.0, 114.5, 115.5, and 118.0 (*from top left to bottom right*) for $\mathrm{Re}_m = 1$ and $\mathrm{Re}_\alpha = 50$. The velocity field is dominated by the azimuthal wavenumber $m = 6$ in the form of progradely traveling waves.

dynamo: the Lorentz force $(\nabla \times \boldsymbol{B}_o) \times \boldsymbol{B}_o$, nonlinear advection of the large-scale flow $\boldsymbol{u} \cdot \nabla \boldsymbol{u}$, and the feedback modulation $\nabla \times (\boldsymbol{u} \times \boldsymbol{B}_o)$. In consequence, the problem of the dynamic interface dynamo is not only more complicated but also requires much more computing resources.

It is of importance to note that, although we impose an axisymmetric profile of α in (25), the resulting dynamic interface dynamo can be either axisymmetric or nonaxisymmetric, depending on which symmetry of the dynamo instability is preferred at given parameters. Moreover, there exist three possible

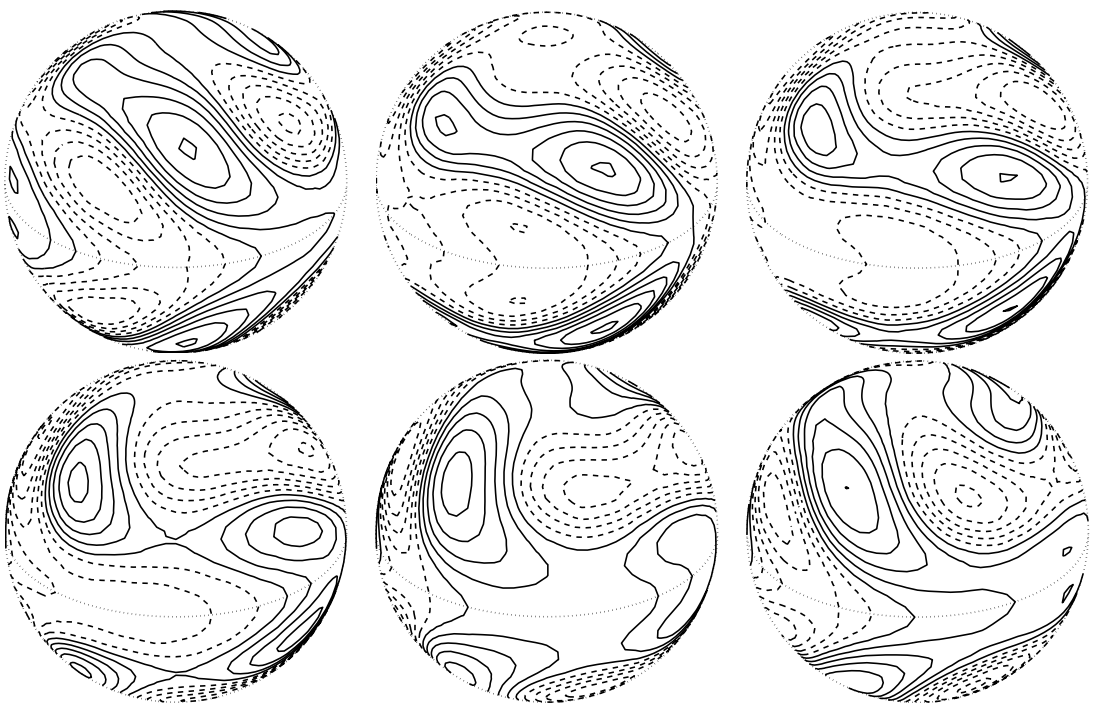

FIG. 6.—Contours of the azimuthal field B_ϕ at the base of convection zone, viewed at an angle of 30° from the axis of rotation and plotted at six different instants, $t = 86.1$, 87.9, 89.1, 90.0, 91.5, and 93.30 (*from top left to bottom right*) for $\mathrm{Re}_m = 5$ and $\mathrm{Re}_\alpha = 50$. The magnetic field is dominated by the azimuthal wavenumber $m = 2$ in the form of progradely traveling dynamo waves.

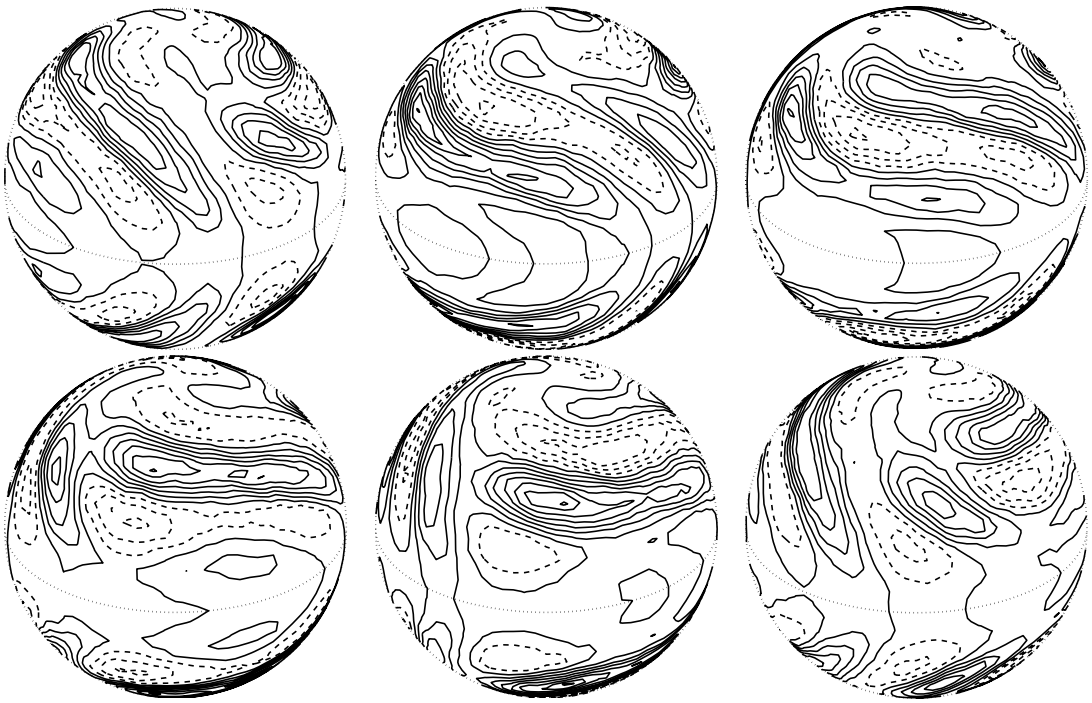

FIG. 7.—Contours of the azimuthal flow u_ϕ at the middle surface of the convection zone, viewed at an angle of 30° from the axis of rotation and plotted at six different instants, $t = 86.1$, 87.9, 89.1, 90.0, 91.5, and 93.30 (*from top left to bottom right*) for $\mathrm{Re}_m = 5$ and $\mathrm{Re}_\alpha = 50$. The velocity field is dominated by the azimuthal wavenumber $m = 4$ in the form of progradely traveling waves.

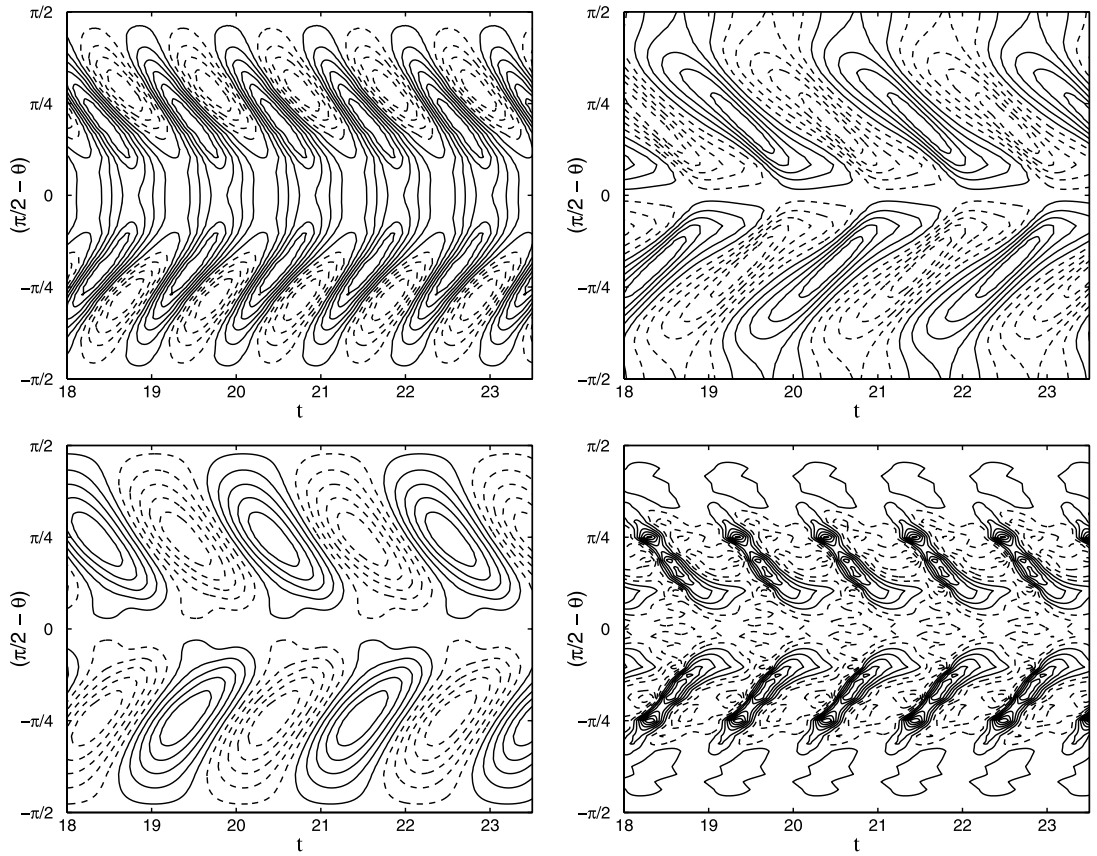

FIG. 8.—Butterfly-type diagram for the azimuthal flow u_ϕ (*top left*) and the radial magnetic field B_r (*top right*) at the middle surface of the convection zone, and for the toroidal magnetic field B_ϕ (*bottom left*) at the base of the convection zone and the radial velocity field u_r (*bottom right*) at the middle surface of the convection zone for $\mathrm{Re}_m = 10$. The solid contours denote the positive values of variables like $B_\phi > 0$, while the dashed contours are for the negative values of variables like $B_\phi < 0$. The dynamic interface dynamo is axisymmetric.

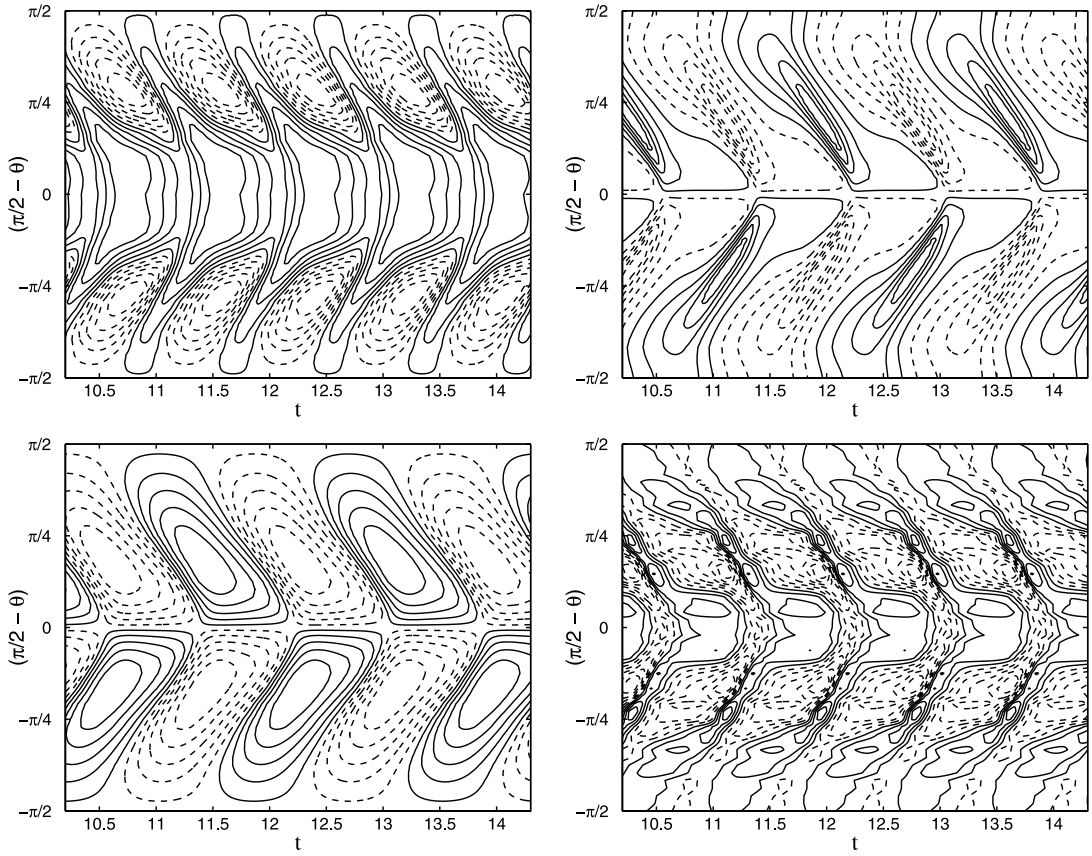

FIG. 9.—Butterfly-type diagram for the azimuthal flow u_ϕ (*top left*) and the radial magnetic field B_r (*top right*) at the middle surface of the convection zone, and for the toroidal magnetic field B_ϕ (*bottom left*) at the base of the convection zone and the radial velocity field u_r (*bottom right*) at the middle surface of the convection zone for $\mathrm{Re}_m = 100$. The dynamic dynamo solution is axisymmetric.

equatorial parities in the generated magnetic field: an equatorially symmetric dynamo with

$$(B_\phi, B_r, B_\theta)(\theta) = (B_\phi, B_r, -B_\theta)(\pi - \theta),$$

an equatorially antisymmetric dynamo with

$$(B_\phi, B_r, B_\theta)(\theta) = (-B_\phi, -B_r, B_\theta)(\pi - \theta),$$

or a dynamic dynamo with mixed equatorial symmetries. Our nonlinear simulation does not impose any azimuthal or equatorial symmetries which are selected only by the physical process of dynamic interface dynamos.

Without having the shearing effect in the tachocline at $\mathrm{Re}_m = 0$, the onset of the dynamic α^2 dynamo occurs at about $\mathrm{Re}_\alpha = 25$. It should be mentioned that, apart from an increase in the amplitude of the nonlinear dynamo, there are no substantial differences in the spatial structure between the $\mathrm{Re}_\alpha = 25$ and 50 dynamo solutions. Since our objective is to understand the basic mechanism of dynamic interface dynamos, we shall fix Re_α at $\mathrm{Re}_\alpha = 50$, which suffices to sustain a weak dynamic α^2 dynamo, and then investigate how the effect of the tachocline alters the dynamo behavior by gradually increasing the magnetic Reynolds number Re_m.

Six different nonlinear solutions of the dynamic interface dynamos obtained at various values of Re_m are presented in Figure 2, showing the magnetic energy E_{mag} and kinetic energy E_{kin} of the dynamos as a function of time, where

$$E_{\mathrm{mag}} = \frac{1}{2V}\int_V |\boldsymbol{B}|^2\, dV, \quad E_{\mathrm{kin}} = \frac{1}{2V}\int_V |\boldsymbol{u}|^2\, dV,$$

where V denotes the region given by $r_i \le r \le r_o$. Several interesting features emerge from the simulations of the dynamic interface dynamo. At first glance, it is surprising that the dynamic interface dynamos at small values of Re_m are more complicated. While the dynamic dynamos with large values of Re_m are simply periodic, the nonlinear solutions for small Re_m are quasi-periodic or nearly irregular. This unusual feature can be explained by looking at the planform of the generated magnetic and velocity field, shown on a spherical surface, for $\mathrm{Re}_m = 1$ in Figures 3–5. It can be seen that the magnetic field generated by the dynamic interface dynamo at $\mathrm{Re}_m = 1$ is nonaxisymmetric, with a dominant azimuthal wavenumber $m = 3$, along with other subdominant wavenumbers, with mixed equatorial symmetries. As a result of the quadratic Lorentz force, the flow velocity, which is primarily driven by the magnetic force, is characterized by the dominant azimuthal wavenumber $m = 6$. The feature that the magnetic energy is greater than the kinetic energy is certainly linked to the α-quenching used in the model and, hence, is of less physical significance.

This temporally and spatially complicated behavior can be attributable to the weak effect of the tachocline. For small Re_m, several dynamo modes with different equatorial parities and

various azimuthal wavenumbers are excited by dynamo instabilities at $\mathrm{Re}_\alpha = 50$. Because of the existence of the large radiative core with a high electric conductivity, the effective communication of the generated magnetic field between the different regions of longitudes is blocked, leading to the preference of nonaxisymmetric dynamic interface dynamos with mixed equatorial symmetries. Moreover, the nonlinear interaction of various modes gives rise to a complex time dependence of the solution. When Re_m increases, it is anticipated that both the scales of the generated magnetic field and the flow will be enlarged. As shown in Figures 6 and 7 for the dynamic interface dynamo at $\mathrm{Re}_m = 5$, the dominant wavenumber for the magnetic field decreases to $m = 2$ which drives a flow with the azimuthal wavenumber $m = 4$.

The possibility of exciting the nonaxisymmetric interface dynamo modes is, however, removed when the magnetic Reynolds number Re_m, which measures the amplitude of the differential rotation in the tachocline, is sufficiently large with $\mathrm{Re}_m \geq O(10)$. In this case, the effective communication of the generated magnetic field between the different regions of longitudes is reestablished by the strong differential rotation, leading to a temporally and spatially simple dynamic interface dynamo. It reenforces the view that the nearly regular cycle of the solar global magnetic activities has to be regularized by a relatively simple large-scale flow, like the differential rotation in the tachocline, that controls the dynamo behavior.

Figure 8 shows contours of the toroidal magnetic field at the interface r_t, the radial flow, the radial magnetic field, and the toroidal flow at the middle of the convection zone, plotted against time, for $\mathrm{Re}_m = 10$, where the solid contours denote the positive values of variables, while the dashed contours are for the negative values of variables. Note that the dynamo solution shown Figure 8 is axisymmetric and therefore independent of the longitude. A similar profile of the magnetic field and the toroidal flow for $\mathrm{Re}_m = 100$ is displayed in Figure 9, revealing that the basic properties of the dynamic interface dynamos remain nearly unchanged. It should be noted that the amplitude of meridional circulation, which typically has a dominant large cell across the equator along with two smaller cells in middle and higher latitudes, is usually about 20% that of the differential rotation. With the stronger effects of the tachocline for $\mathrm{Re}_m \geq O(10)$, we found that (1) the action of the strong tachocline always produces an oscillatory dynamic dynamo with a period of about two magnetic diffusion units; (2) the multilayered dynamic interface dynamos also produce a torsional oscillation of the azimuthal flow propagating toward the equator with a period of about one magnetic diffusion unit; (3) the dynamic dynamo is always axisymmetric, selects dipolar symmetry, and propagates equatorward, even though the simulation is fully three-dimensional; and (4) the generated magnetic field mainly concentrates in the vicinity of the interface between the tachocline and the convection zone.

3.2. *Dynamic Dynamos with 3D α-Effects*

The observation of the solar magnetic field suggests that the solar dynamo may be nonaxisymmetric, characterized by magnetic activities in persistent different longitudes, and the total number of active regions per rotation per hemisphere varied between zero and seven (e.g., De Toma et al. 2000). It was also argued that the number of persistent bands of magnetically active nests in the observed solar magnetic fields corresponds to the longitudinal wavenumber m in the magnetic field, which is $m = O(1)$. The simplest way to generate a nonaxisymmetric magnetic field is to employ a nonaxisymmetric α-distribution in the mean field dynamo framework (Rüdiger 1980; Moss & Brandenburg 1995). For the purpose of understanding the basic mechanism of nonaxisymmetric dynamic interface dynamos, we consider the dynamic interface dynamo with a nonaxisymmetric α-distribution in the form

$$\alpha = \sin^2\theta\cos\theta(1+\epsilon\cos M\phi) \times \sin\left[\pi\frac{(r-r_t)}{(r_o-r_t)}\right]\frac{1}{\left(1+|\boldsymbol{B}_o|^2\right)}, \quad r_t < r \leq r_o, \qquad (26)$$

where $\epsilon = 0$ recovers the axisymmetric case and M is an azimuthal wavenumber treated as a parameter. In our numerical simulations, we take $\epsilon = 0.75$ and $M = 1$, while the value of Re_α is still fixed at 50.

It should be pointed out that, as a result of the prescribed nonaxisymmetric α-effect, purely axisymmetric dynamic interface dynamos are no longer feasible: all resulting dynamic interface dynamos must be nonaxisymmetric. Five solutions of the dynamic interface dynamos obtained at various values of Re_m are presented in Figure 10, showing the magnetic energy E_{mag} and kinetic energy E_{kin} of the dynamo solutions as a function of time. Two new types of the interface dynamos are found: azimuthally traveling hemispherical dynamos and equatorwardly propagating nonaxisymmetric dynamos. When the effect of the differential rotation in the tachocline is not sufficiently strong for

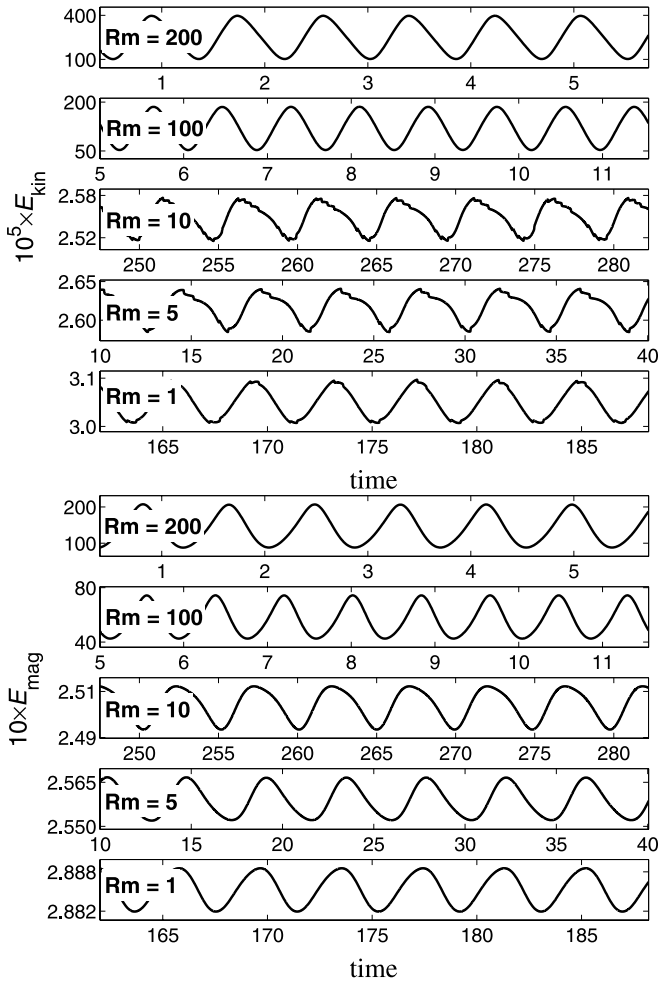

FIG. 10.—Kinetic energy E_{kin} (*top*) and magnetic energy E_{mag} (*bottom*) as a function of time for five different dynamo solutions with different values of Re_m. The profile of the prescibed α is three-dimensional in the convection zone.

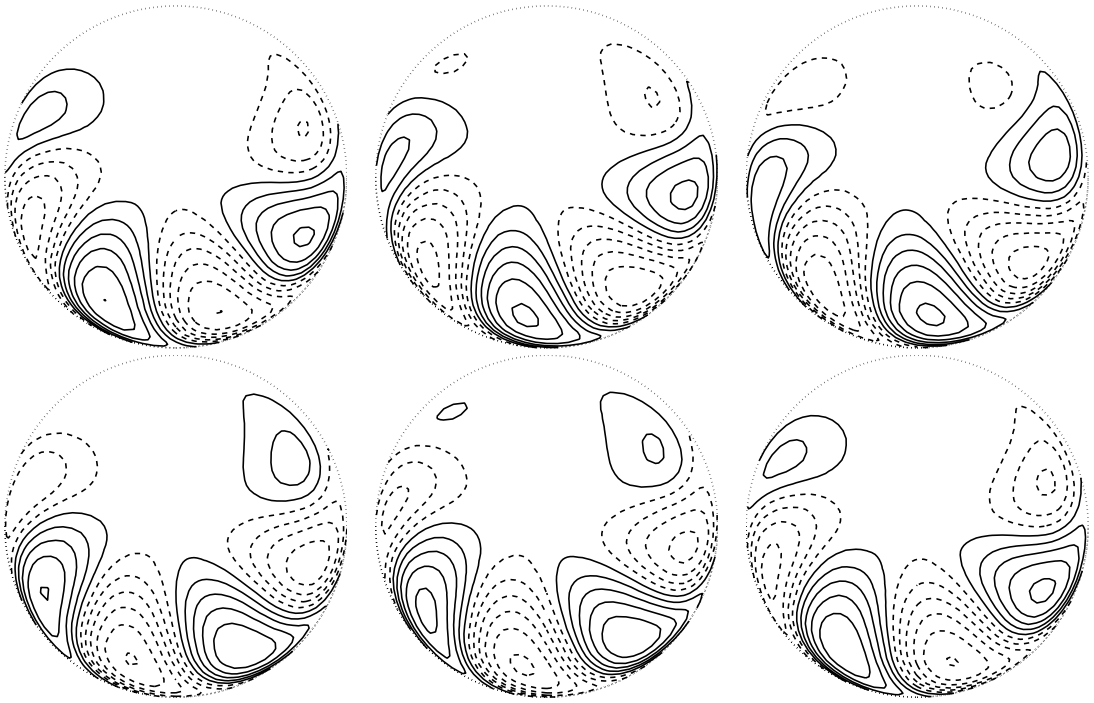

FIG. 11.—Contours of the azimuthal field B_ϕ at the base of the convection zone, viewed from the north pole and plotted at six different instants, $t = 270.0, 272.0, 273.6, 276.0, 276.8$, and 279.6 (*from top left to bottom right*) for $\mathrm{Re}_m = 10$ and $\mathrm{Re}_\alpha = 50$. The magnetic field is dominated by the azimuthal wavenumber $m = 4$ and concentrates largely in one hemisphere.

$\mathrm{Re}_m \leq O(10)$, the magnetic field and the corresponding flow are primarily confined within a hemisphere defined approximately by the longitudes $-\pi/2 < \phi < \pi/2$, which are illustrated in Figures 11 and 12. It shows that the magnetic field generated by the dynamic interface dynamo is strongly nonaxisymmetric with a dominant azimuthal wavenumber $m = 4$. Driven by the quadratic Lorentz force, the flow is characterized by the dominant azimuthal wavenumber $m = 8$. A particularly interesting feature is that the dynamic interface dynamo, due to the moderate effect of the differential rotation in the tachocline in this case, is in the form of an azimuthally traveling dynamo wave. However, when the dynamo wave travels toward the vicinity of the boundary between the nondynamo hemisphere and the dynamo hemisphere, it disappears.

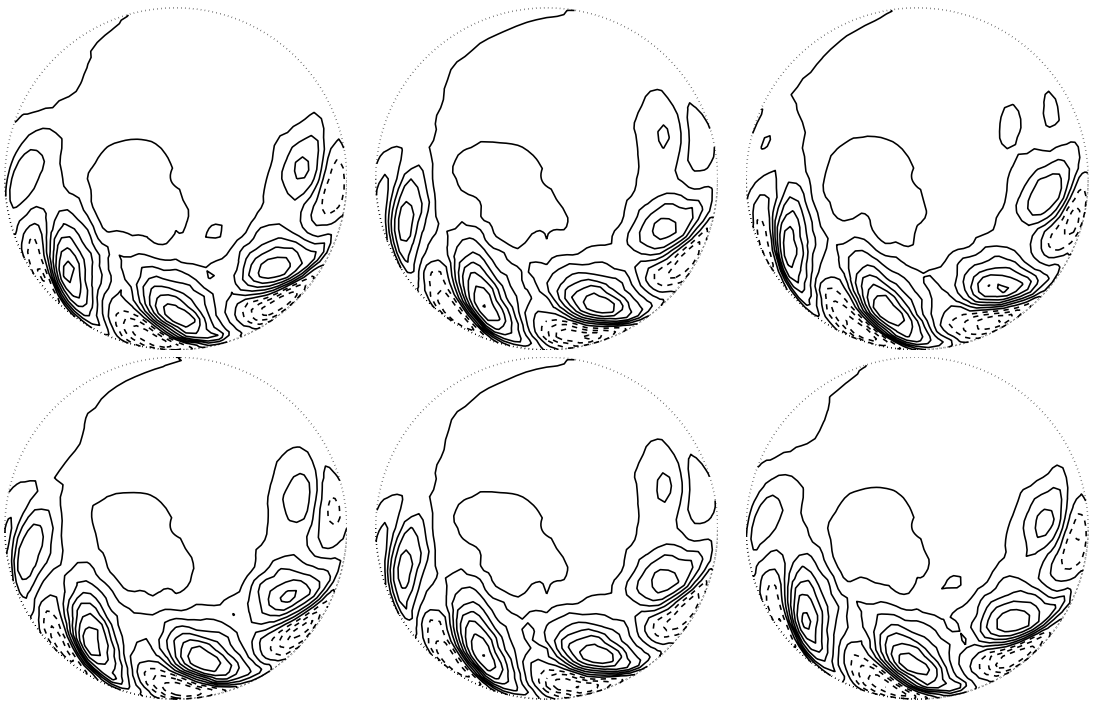

FIG. 12.—Contours of the azimuthal flow u_ϕ at the middle surface of the convection zone, viewed from the north pole and plotted at six different instants, $t = 270.0, 272.0, 273.6, 276.0, 276.8$, and 279.6 (*from top left to bottom right*) for $\mathrm{Re}_m = 10$ and $\mathrm{Re}_\alpha = 50$. The velocity field is dominated by the azimuthal wavenumber $m = 8$ and concentrates largely in the hemisphere where dynamo action exists.

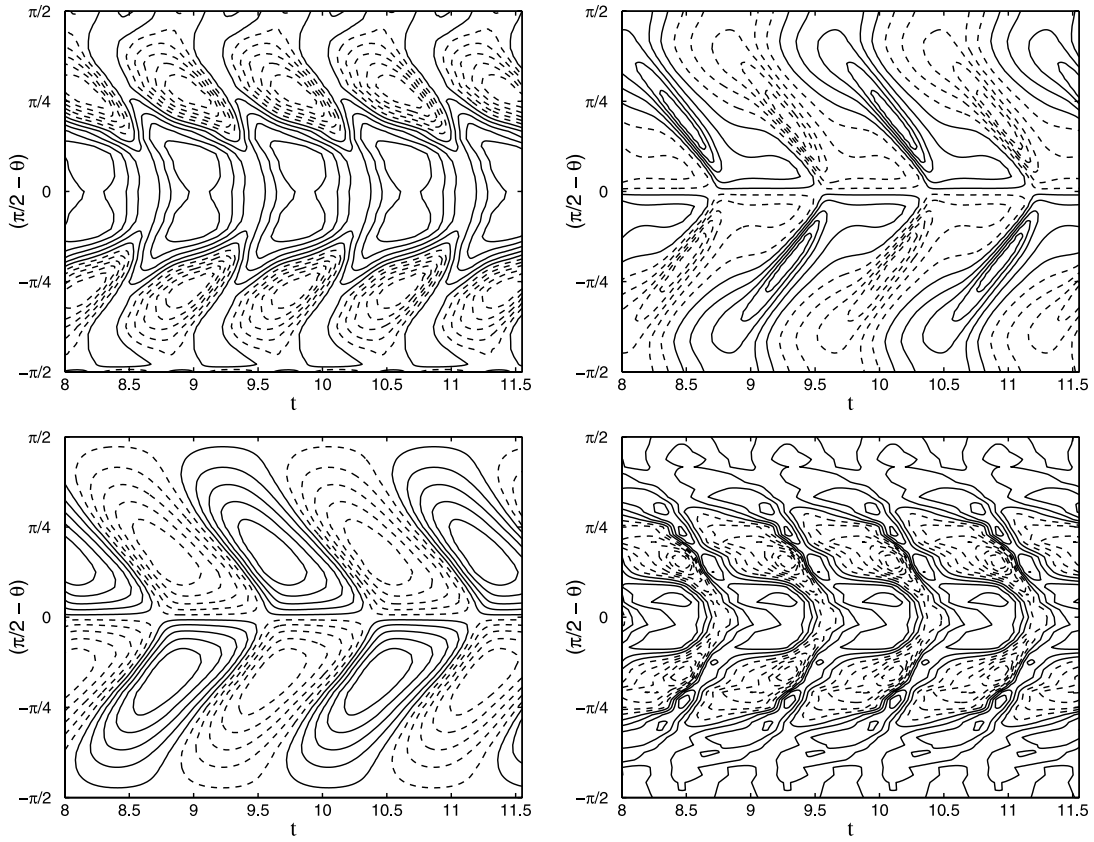

FIG. 13.—Butterfly-type diagram for the azimuthal flow u_ϕ (*top left*) and the radial magnetic field B_r (*top right*) at the middle surface of the convection zone, and for the toroidal magnetic field B_ϕ (*bottom left*) at the base of the convection zone and the radial velocity field u_r (*bottom right*) at the middle surface of the convection zone at a fixed longitude $\phi = \pi/2$ for $\mathrm{Re}_m = 100$. The dynamic interface dynamo is nonaxisymmetric and oscillatory and propagates toward the equator.

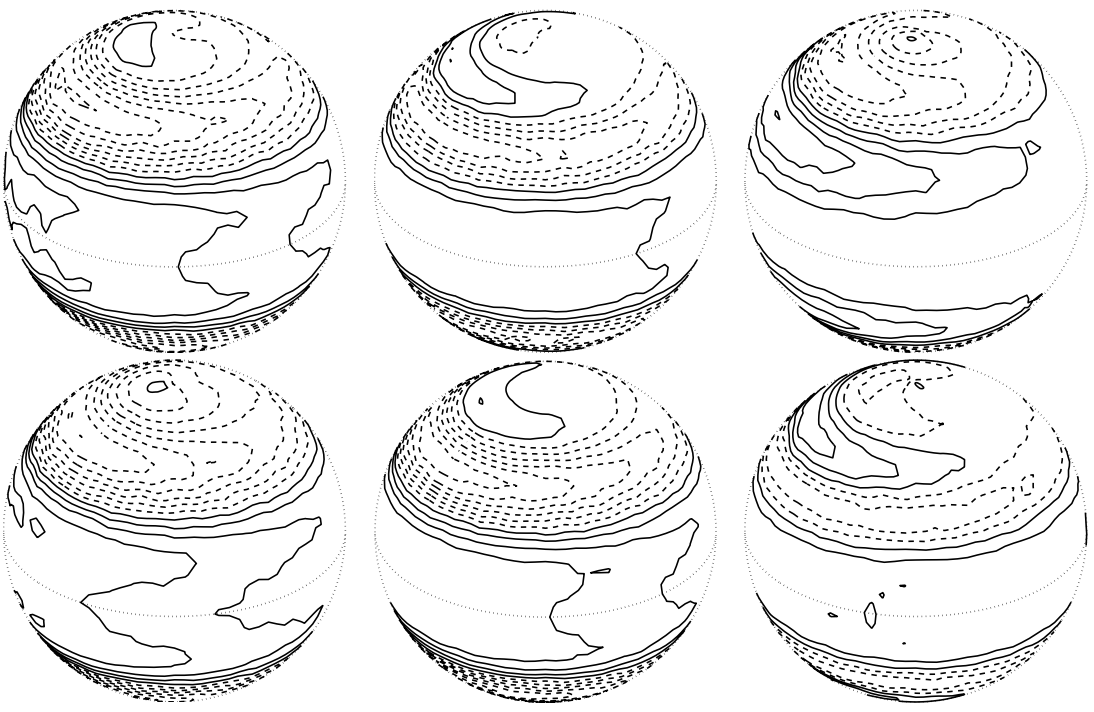

FIG. 14.—Contours of the azimuthal flow u_ϕ at the middle surface of the convection zone, viewed at an angle of 30° from the axis of rotation and plotted at six different instants, $t = 9.8$, 10.0, 10.3, 10.5, 10.7, and 10.9 (*from top left to bottom right*) for $\mathrm{Re}_m = 100$ and $\mathrm{Re}_\alpha = 50$.

The azimuthally traveling wave hemispherical dynamo is switched to an equatorward propagating dynamo wave when the effect of the tachocline becomes strong and dominant. For $\mathrm{Re}_m \geq O(100)$, the interface dynamic dynamos are still nonaxisymmetric, but in the form of equatorwardly propagating dynamo waves. Figure 13 shows contours of the toroidal magnetic field at the interface r_t and the radial magnetic field and the azimuthal flow at the middle of the convection zone, plotted against time, for $\mathrm{Re}_m = 10$ in a fixed meridional plane. It is shown that both the nonaxisymmetric dynamic dynamo wave and the corresponding torsional oscillation propagate toward the equator. The time-dependent structure of the generated toroidal flow is displayed in Figure 14: the toroidal flow is strongest at a particular longitude where there exist strong magnetic activities in that region.

Although the dynamic interface dynamos are always nonaxisymmetric, our results again underscore the importance of the tachocline that controls the style of a dynamic interface dynamo. A strong action of the tachocline is required to produce the oscillatory magnetic field and the torsional oscillating flow that, even though they are nonaxisymmetric, select dipolar symmetry, and propagate equatorward.

4. SUMMARY AND REMARKS

As an important step in our effort to construct a three-dimensional finite-element solar dynamo model, this study has followed the idea of Parker's interface dynamo by separating the α- and ω-processes spatially, an essential ingredient in an interface dynamo. Our dynamic interface dynamo model consists of four regions which are coupled magnetically through the matching conditions at the interfaces. By gradually increasing the strength of the differential rotation in the tachocline, we have investigated a nonlinear, time-dependent, spherical dynamic interface dynamo using a finite-element method based on the three-dimensional tetrahedralization of the spherical system. However, we did not perform fully nonlinear MHD simulations. In the convection zone, although the fully three-dimensional feedback of the Lorentz force has been taken into account, the Malkus-Proctor formulation with a prescribed α-effect is employed without explicitly including the effect of thermal convection. Moreover, the dynamic feedback on the prescribed shear flow in the tachocline is totally neglected.

This paper represents the first study on the three-dimensional, multilayered dynamic interface dynamo taking the fully three-dimensional feedback of the Lorentz force in the convection zone, in an attempt to understand the basic mechanism of the interface dynamo rather than simulating realistic solar magnetic fields. We find that, when Re_m is sufficiently large, the action of the shear confined within the tachocline always produces oscillatory dynamos with a period of about two magnetic diffusion units, which is about 20 yr if the magnetic diffusivity in the convection zone is taken as $10^8\ \mathrm{m}^2\ \mathrm{s}^{-1}$. The corresponding torsional oscillation of the flow has a period of about one magnetic diffusion unit, which corresponds to about 10 yr. All our nonlinear dynamic simulations for $\mathrm{Re}_m \geq O(100)$ suggest that, whether the α-effect is two- or three-dimensional, the dynamic interface dynamo is always axisymmetric or predominantly axisymmetric, selects dipolar symmetry, and propagates equatorward. Without the controlling effect of strong regular shears in the tachocline, the behavior of dynamic interface dynamos becomes, both temporally and spatially, much more complicated. A convection-driven EBE finite-element solar dynamo is currently under construction which will consider the thermal effect and the coupling of the Navier-Stokes and dynamo equations everywhere, including the radiative core and tachocline. But this will be a very difficult problem because we do not know how and why the tachocline is formed, without which it is unlikely that a solar-like dynamo solution will be produced.

The hemispherical dynamo—where one hemisphere within the longitudes $-\pi/2 < \phi < \pi/2$ has an active dynamo, while there is no dynamo action in the other hemisphere $\pi/2 < \phi < 3\pi/2$—may be relevant to the dynamo action taking place in the Pegasus B-type extrasolar giant planets (see, e.g., Seager & Sasselov 1998; Showman & Guillot 2002). This type of extrasolar planet is characterized by being a short distance from its parent star, usually less than $O(0.1\ \mathrm{AU})$, and, consequently, strong tidal interactions between the planet and parent star quickly bring the planet into synchronized rotation with the parent star. In this case, we would expect the large hemispherical difference between its hotter day side constantly penetrated by strong stellar radiation and its cold night side.

X. L. is supported by NSFC grant/10633030 and CAS grant/KJCX2 YW T13 and K. Z. is supported by UK NERC and PPARC grants. Computation is supported by Shanghai Supercomputer Center.

REFERENCES

Brandenburg, A. 2001, ApJ, 550, 824
Brandenburg, A., Moss, D., & Tuominen, I. 1992, A&A, 265, 328
Brandenburg, A., & Subramanian, K. 2005, Phys. Rep., 417, 1
Browning, M. K., Miesch, M. S., Brun, A. S., & Toomre, J. 2006, ApJ, 648, L157
Brun, A. S., & Toomre, J. 2002, ApJ, 570, 865
Bushby, P. J. 2003, MNRAS, 342, L15
Cameron, R., & Schüssler, M. 2007, ApJ, 659, 801
Cattaneo, F. 1999, ApJ, 515, L39
Chan, K. H., Zhang, K., Li, L., & Liao, X. 2007, Phys. Earth Planet. Inter., 163, 251
Chan, K. H., Zhang, K., Zou, J., & Schubert, G. 2001, Phys. Earth Planet. Inter., 128, 35
Charbonneau, P. 2005, Living Rev. Sol. Phys., 2, 2
Charbonneau, P., & MacGregor, K. B. 1997, ApJ, 486, 502
Choudhuri, A. R., Schüssler, M., & Dikpati, M. 1995, A&A, 303, L29
Cline, K. S., Brummell, N. H., & Cattaneo, F. 2003, ApJ, 599, 1449
Covas, E., Tavakol, R., & Moss, D. 2001, A&A, 371, 718
De Toma, G., White, O. R., & Harvey, K. L. 2000, ApJ, 529, 1101
Dikpati, M., & Charbonneau, P. 1999, ApJ, 518, 508
Dikpati, M., de Toma, G., & Gilman, P. A. 2006, Geophys. Res. Lett., 33, L05102
Dikpati, M., & Gilman, P. A. 2006, ApJ, 649, 498
Glatzmaier, G. A., & Gilman, P. 1982, ApJ, 256, 316
Kitchatinov, L. L., & Rüdiger, G. 1995, A&A, 299, 446
Kosovichev, A. G. 1996, ApJ, 469, L61
Küker, M., Rüdiger, G., & Schultz, M. 2001, A&A, 374, 301
Liao, X., & Zhang, K. 2006, ApJ, 638, L113
Liao, X., Zhang, K., & Chang, Y. 2007, Phys. Rev. Lett., 98, 094501
MacGregor, K. B., & Charbonneau, P. 1997, ApJ, 486, 484
Malkus, W. V. R., & Proctor, M. R. E. 1975, J. Fluid Mech., 67, 417
Markiel, J. A., & Thomas, J. H. 1999, ApJ, 523, 827
Miesch, M. S., Brun, A. S., DeRosa, M. L., & Toomre, J. 2008, ApJ, 673, 557
Moss, D., & Brandenburg, A. 1995, Geophys. Astrophys. Fluid. Dyn., 80, 229
Parker, E. N. 1993, ApJ, 408, 707
Rempel, M. 2006a, ApJ, 637, 1135
———. 2006b, ApJ, 647, 662
Rüdiger, G. 1980, Astron. Nachr., 301, 181
Schou, J., et al. 1998, ApJ, 505, 390
Seager, S., & Sasselov, D. D. 1998, ApJ, 502, L157
Showman, A. P., & Guillot, T. 2002, A&A, 385, 166
Spruit, H. C. 2002, A&A, 381, 923
Tobias, S. M. 1997, A&A, 322, 1007
Weiss, N. O. 1994, in Lectures on Solar and Planetary Dynamos, ed. M. R. E. Proctor & A. D. Gilbert (Cambridge: Cambridge Univ. Press), 59
Zahn, J.-P., Brun, A. S., & Mathis, S. 2007, A&A, 474, 145
Zhang, K., Chan, K. H., Zou, J., Liao, X., & Schubert, G. 2003, ApJ, 596, 663
Zhang, K., & Schubert, G. 2006, Rep. Prog. Phys., 69, 1581